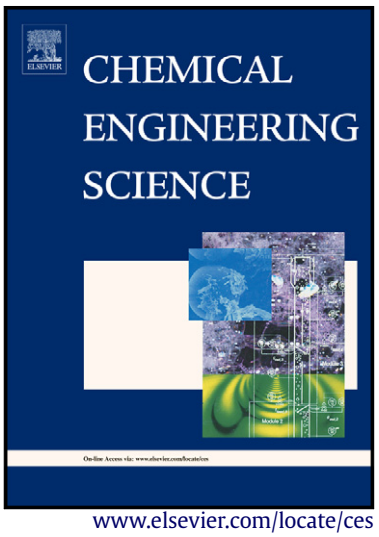

Investigation of a swirling flow nozzle for a fluidised BEd gas distributor

Samson M. Aworinde, Daniel J. Holland, John F. Davidson

www.elsevier.com/locate/ces

PII: S0009-2509(15)00238-9
DOI: http://dx.doi.org/10.1016/j.ces.2015.04.001
Reference: CES12266

To appear in: *Chemical Engineering Science*

Received date: 30 January 2015
Revised date: 30 March 2015
Accepted date: 2 April 2015

Cite this article as: Samson M. Aworinde, Daniel J. Holland, John F. Davidson, Investigation of a swirling flow nozzle for a fluidised BEd gas distributor, *Chemical Engineering Science,* http://dx.doi.org/10.1016/j.ces.2015.04.001

Investigation of a swirling flow nozzle for a fluidised bed gas distributor

Samson M. Aworinde[a,*], Daniel J. Holland[b], John F. Davidson[a]

[a] *Department of Chemical Engineering and Biotechnology, University of Cambridge, Pembroke Street, Cambridge, CB2 3RA, United Kingdom*

[b] *Department of Chemical and Process Engineering, University of Canterbury, Christchurch, New Zealand*

Abstract

This paper relates to a multi-orifice distributor for a gas-fluidised bed, using many upward-facing nozzles, equally spaced in a horizontal plate. Each orifice contained a removable helical coil, which made the gas swirl as it entered the bed. For a single orifice in such a distributor, ultra-fast magnetic resonance imaging (MRI) and pressure measurements were applied to study: (*i*) the formation of jets and bubbles, and (*ii*) the orifice pressure drop. Results from MRI show that the swirling flow induced by the helix significantly improves the fluidisation quality compared to a plain nozzle without spiral. The helix gives rise to secondary flow which increases pressure drop across the nozzle, the measured values of which are predicted satisfactorily by using a friction factor correlation for helical coils.

Keywords: Fluidised bed; Gas distributor; Hydrodynamics; Swirling flow; Pressure drop; Magnetic resonance imaging (MRI)

1. Introduction

1.1. *Fluidised bed and design of gas distributor*

The performance of a fluidised bed is intimately linked to the design of the gas distributor since this influences the efficiency of gas-solid mixing, jet formation, the size and shape of gas bubbles as well as the pressure drop across the distributor. The role of the distributor is to disperse uniformly the fluidising gas over the entire cross-section of the bed and hence to initiate effective gas-solid contacting. Poor design of the distributor can cause severe gas bypassing resulting in channelling and non-uniform fluidisation. Despite various approaches aimed at improving gas-solid contact in fluidised beds, including flow pulsation (Koksal and Vural 1998), vibration (Mawatari, Tatemoto, and Noda 2003), mechanical agitation (Kim and

* Corresponding author. Tel.: +44 1223 334 777
E-mail address: sma48@cam.ac.uk (S.M. Aworinde).

Han 2006), and the use of a rotating distributor (Sobrino et al. 2009; De Wilde and de Broqueville 2008), the effect of the gas distributor design on the bed hydrodynamics is still poorly understood. The limitation of the aforementioned arrangements is that none of them appears suitable for a large industrial fluidised bed unit unlike the helical spiral nozzle investigated in the present paper, which has been used successfully in industrial-scale applications (Kleinfelder 1969; Dunn 1958). A number of studies have investigated an annular spiral distributor made of overlapping angled blades which produces a swirl motion of the bed material (Sreenivasan and Raghavan 2002; Chyang and Lin 2002; Shu, Lakshmanan, and Dodson 2000; Ouyang and Levenspiel 1986); this concept has found use in industrial equipment such as the 'torbed' process reactor technology but the design is very different to the helical spiral nozzle distributor in this work. To the best of our knowledge there has been no published work on the helical nozzle distributor concept in the literature.

1.2. *Magnetic resonance imaging of fluidised beds*

The study of granular systems such as fluidised beds often involves difficult measurements due to the optically opaque nature of the media. This makes it difficult to observe the behaviour of gas and solids within the bulk of the bed. Some of the early experimental techniques that have been applied to study the dynamic behaviour of gas and solid particles in a fluidised bed include capacitance probes (Werther 1974), visual observation (Merry 1975), x-ray photography (Rowe 1971), light probes (Wen, Deole, and Chen 1982) and electroresistivity probes (Choi, Son, and Kim 1988). The major limitation of the probes is that they are intrusive and tend to distort the flow.

More recently, other techniques have been developed, which include positron emission particle tracking (Stein et al. 1997), electrical capacitance tomography (Dyakowski et al. 1997), particle imaging velocimetry (Chen and Fan 1992), diffusing wave spectroscopy (Menon 1997), and magnetic resonance imaging (Müller et al. 2008; Mantle et al. 2008; Pore et al. 2010). Of these techniques, MRI has emerged as a powerful tool for studying visually opaque 3-D systems of two-phase flow. It can provide both ultra-fast as well as time-averaged measurements of the distribution of gas and solids, which makes it useful for studying the phenomena of jets, bubbles, and slugs in fluidised beds and other multi-phase flows. MRI enables the imaging of gas-solid fluidised beds to high spatial and temporal resolutions. Furthermore, MRI allows direct measurement of particle distribution (i.e. voidage) as well as particle velocities, which can be used to identify dead-zones within the bed (Pore et al. 2012).

The aim of this paper is to investigate a novel fluidised bed gas distributor. The distributor plate contains many upward-facing nozzles, each of which is a vertical pipe incorporating a helical coil that makes the gas swirl as it enters the bed. A model of this distributor design was built with a single nozzle containing a helix, replicating the full-scale design. An MRI technique was used to study the flow patterns in the region above the distributor in order to answer the following questions:

i. What is the effect of the swirl on the flow pattern, jet penetration and bubble properties (size and frequency of formation) as the gas enters the fluidised bed and how does bed hydrodynamics compare with a nozzle distributor without swirl?

ii. What is the effect of the helix design on pressure drop across the distributor? How does the pressure drop relate to the gas velocity through the nozzle?

2. Experimental

2.1. *Fluidisation column with swirling flow nozzle distributor*

A schematic diagram of the fluidisation column made of polyether ether ketone (PEEK) is shown in Fig. 1. It consists of a 50 mm diameter distributor plate containing 61 holes, each 0.4 mm diameter, arranged in three evenly spaced concentric circles as well as a 10 mm diameter central nozzle containing a 5 mm diameter rod with a six-turn helical coil at the top. The helix is designed to make the inlet gas swirl as it enters the bed and to retain particles when the fluidising air is switched off. The vertical height of the spiral in the nozzle can be adjusted up or down, or it can altogether be removed to give a simple nozzle without swirl. Without the spiral helix, the arrangement has some similarity to a spout-fluid bed (Mathur and Epstein 1974). On the side of the bed at the gas inlet into the nozzle is a pressure tapping to measure the pressure drop across the helix with respect to the top of the distributor. Fluidising air is supplied through two inlets, one to the main bed and the other to the nozzle containing the helix. The nozzle containing the helix was connected via two Roxspur Platon NGX rotameters (2-25 L/min and 10-100 L/min), calibrated using the soap film method, to the main air supply at 1 bar.

2.2. *Magnetic resonance imaging*

2.2.1. *Materials and MRI system*

For this study, poppy seeds (diameter 500 μm; density ~950 kg/m^3; measured minimum fluidisation velocity, U_{mf}, 0.13 m/s corresponding to a distributor flow rate of 15.3 L/min; Geldart Group B particles (Geldart 1973)) were used for MRI experiments because the

oilseed particles contain ^{1}H nuclei and have relaxation times that provide a favourable signal when using magnetic resonance.

The fluidised bed was contained in a 50 mm I.D. acrylic tube placed vertically within the MRI spectrometer. The main bed, with a settled depth of 150 mm, was vigorously fluidised by passing air at ambient conditions (1 bar and 20 ^{o}C), metered *via* the rotameter, through both the holes in the distributor plate and the nozzle containing the helix. The air was humidified to eliminate the effects of static electricity that may cause particles to stick to the bed walls. The bed was fluidised vigorously for 2 to 3 minutes for the system to become uniform, ensuring reproducibility. Thereafter, flow through the perforated plate (i.e. main bed) was shut off and the nozzle flow decreased to 20 L/min. Flow through the nozzle was then decreased in steps of 2 L/min while magnetic resonance images of the bed were acquired after a steady flow was achieved. Three different layouts of the fluidised bed were studied *i*) nozzle with helix flush with the top of the distributor, *ii*) nozzle with helix lowered to about 27.5 mm below the top of the distributor, *iii*) plain nozzle with the helix removed. Since the radial clearance between the spiral insert and the nozzle wall is smaller than the particle size and the fluidising gas has a relatively high velocity along the spiral, no down-flow of particles past the first helical turn or clogging of the spiral was experienced.

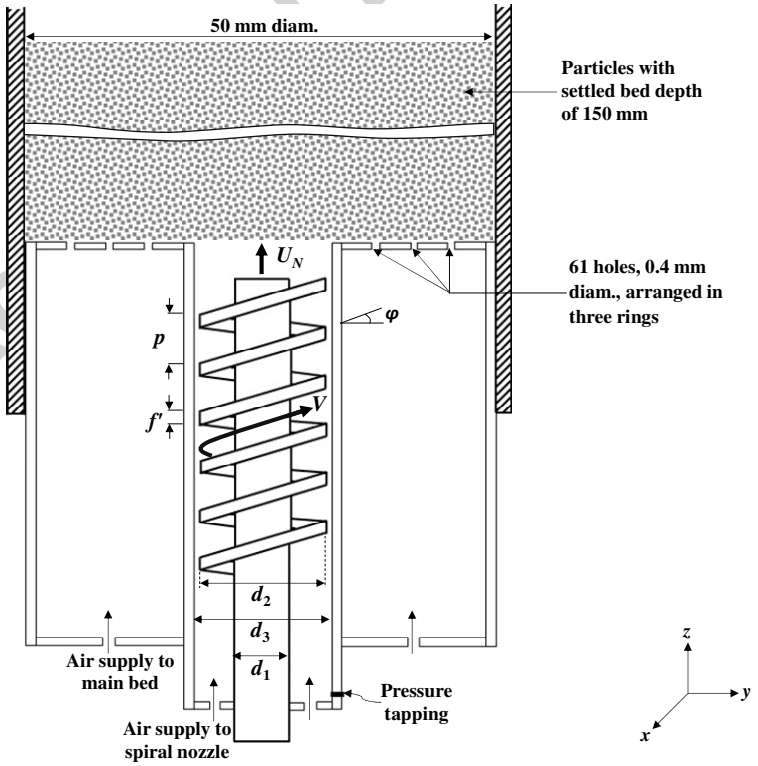

Fig. 1. Schematic representation of the fluidisation column showing the spiral nozzle gas distributor.

Table 1: Geometric parameters of the helical spiral.

Parameter	Value
Number of turns, n	6
Flight, f'	0.65 mm
Pitch, p	4 mm
Core diameter, d_1	5 mm
Outer diameter, d_2	9.8 mm
Central nozzle diameter, d_3	10 mm
Inclined angle, φ	11.5°

Imaging was performed at a proton (^{1}H) frequency of 199.7 MHz on a Bruker DMX 200 MRI spectrometer. A 64 mm I.D. birdcage radio frequency (r.f.) coil enclosing the fluidised bed was used to excite and detect signals from the seed particles. Spatial resolution was achieved using a three dimensional shielded gradient system capable of producing a maximum magnetic field gradient of 0.136 T/m. Three different techniques were employed in each case for the imaging.

2.2.2. *Fast Low Angle Shot (FLASH) imaging*

An ultra-fast imaging sequence based on Fast Low Angle Shot (FLASH) was used to study the transient behaviour of the bed. The FLASH or snapshot images were acquired as a time series of 50 2D images. A slice of 5 mm thickness passing through the axis of symmetry of the bed was imaged with an acquisition time of 26.5 ms per frame and subsequent frames acquired in immediate succession giving a total acquisition time of 1.33 s. Imaging was achieved using 32 × 16 pixels with a field of view of 60 mm × 70 mm in the *x-z* plane resulting in a spatial resolution of 1.9 mm × 4.4 mm. Repetition time T_R (the time between successive excitations of the same slice) and echo time T_E (the time between exciting the sample and the peak of the acquired echo signal) were 1.65 ms and 1.1 ms, respectively.

2.2.3. *Rapid Acquisition with Relaxation Enhancement (RARE) pulse sequence*

The RARE pulse sequence was used to image the jet formation in the *x-z* plane with a field of view of 60 mm × 70 mm and 128 × 128 pixels. This technique was used because it gives better resolution images for the gas jets formed in the bed compared to the FLASH technique.

However it is susceptible to artefacts when particles are moving quickly and so does not produce reliable images under bubbling conditions.

2.2.4. *Multi-Slice Spin Echo Pulse Sequence imaging*

A multi-slice spin-echo pulse sequence was used to obtain intensity maps of the solids at different heights above the distributor. Stacks of 50 adjacent 2D images were acquired in the horizontal (x-y) plane at 1 mm intervals in the z direction. The images were acquired with a T_R of 730 ms and T_E of 2.6 ms, with two averages per slice resulting in a total acquisition time of ~8 minutes for the entire stack of images. The field of view was 60 mm × 60 mm with 128 × 128 pixels resulting in a spatial resolution of 0.47 mm × 0.47 mm.

2.3. *Pressure drop measurement*

The fluidised bed was maintained in a vertical position on a retort stand without particles on the distributor i.e. open to the atmosphere. A digital pressure meter (Digitron Instrumentation, Model P100H) was connected to the pressure tapping located at the entrance to the nozzle to measure the pressure drop with respect to the atmosphere. Air flow rates through the nozzle ranged from 0 L/min to 60 L/min corresponding to nozzle gas velocity, U_N, up to 12.73 m/s. The pressure drop between the bottom of the nozzle and the top of the distributor was measured with the helix in the flush and lowered positions and also without the helix in place.

3. Theory

3.1 *Definition of jet and bubble*

Fig. 2 shows the illustration of a jet and bubble in a fluidised bed with typical geometrical properties.

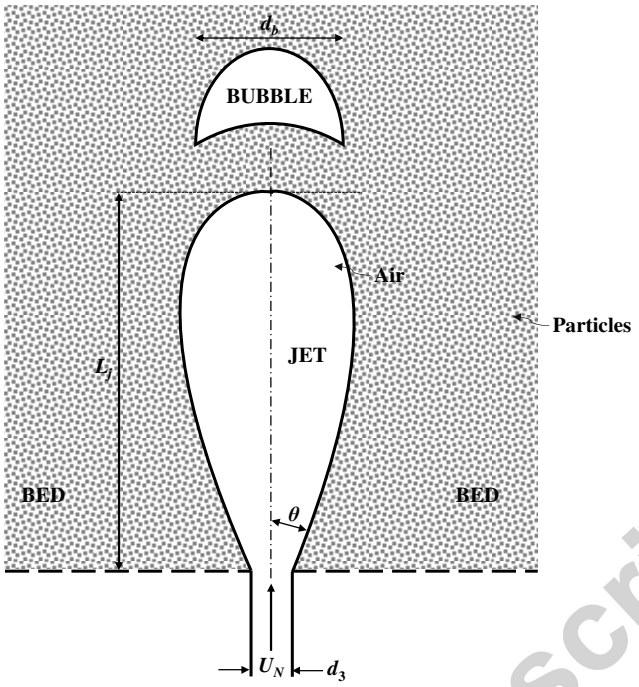

Fig. 2. Geometrical properties of an axisymmetric jet and bubble in a fluidised bed.

Correlations (Merry 1975) for vertical jet penetration length (L_j) and bubble diameter (d_b) are:

$$\frac{L_j}{d_3} = 5.2\left(\frac{\rho_g d_3}{\rho_p d_p}\right)^{0.3}\left[1.3\left(\frac{U_N^2}{g d_3}\right)^{0.2} - 1\right] \quad (1)$$

$$(d_b / d_3) = 0.33(U_N^{0.4} / d_3^{0.2}) \quad (2)$$

where d_3 is the nozzle diameter and U_N is the gas velocity through the nozzle as shown in Fig. 1. Other symbols are defined in the notation list.

3.2. *Pressure drop across the spiral nozzle*

In addition to jet and bubble characteristics, the pressure drop across a fluidised bed gas distributor is of paramount importance in industrial applications since this affects the behaviour and performance of the bed. Too low distributor pressure drop may result in maldistribution of gas leading to poor fluidisation while too high pressure drop will increase operating costs.

When a fluid flows through a helical channel or curved pipe, a secondary flow pattern acting perpendicular to the main flow is induced by the centrifugal forces generated by the curvature (Dean 1927; Thomson 1876). The secondary flow changes the fluid behaviour and hence frictional loss leading to a higher pressure drop in the helix. Another effect of the secondary

flow is the stabilization of flow, giving a significant increase in the Reynolds number for the transition from laminar to turbulent flow (Thangam and Hur 1990). Thus, the flow is different from that in a straight pipe, and the pressure drop across the helical channel is calculated using friction factor correlations for helical coils.

Taking a vertical section through the nozzle (Fig. 1) the nozzle volumetric gas flow is

$$Q_N = V\cos\varphi(p - f')(d_3 - d_1)/2 \tag{3}$$

where V is the tangential velocity of the gas in the nozzle and the dimensions p, f', d_3 and d_1 are shown in Fig. 1.

In terms of the superficial nozzle velocity, U_N, the flow rate is

$$Q_N = (\pi/4)d_3^2 U_N \tag{4}$$

Combining Eqs. (3) and (4) gives the swirl velocity

$$V = \frac{\pi}{2}\frac{U_N d_3^2}{(d_3 - d_1)(p - f')\cos\varphi} \tag{5}$$

Important geometric parameters that characterise the helical channel cross section include the helix length l, the flow area A, periphery (wetted perimeter) P', the number n, of turns in the helix, and the hydraulic diameter d_H, which are related by

$$l = \pi n(d_1 + d_2)/2 \tag{6}$$

$$A = (p - f')\cos\varphi(d_3 - d_1)/2 \tag{7}$$

$$P' = 2(p - f')\cos\varphi + (d_3 - d_1) \tag{8}$$

$$d_H = \frac{4A}{P'} = \frac{2(p - f')(d_3 - d_1)\cos\varphi}{2(p - f')\cos\varphi + (d_3 - d_1)} \tag{9}$$

The pressure drop across the swirling flow nozzle is a combination of the effect of friction along the nozzle (given by the Darcy-Weisbach equation) and the entry loss in the nozzle, giving

$$\Delta P = f\frac{2l}{d_H}\rho_g V^2 + \frac{1}{2}\rho_g V^2 \tag{10}$$

where f is the Fanning friction factor for the helical coil.

Putting Eq. (5) into Eq. (10) and rearranging gives the total pressure drop

$$\Delta P = \left(0.5 + \frac{2fl}{d_H}\right)\left[\frac{\pi d_3^2}{2(d_3 - d_1)(p - f')\cos\varphi}\right]^2 \rho_g U_N^2 \tag{11}$$

The Blasius equation (Blasius 1913) is used for calculating the friction factor in straight channels and is

$$f = 0.079\,\mathrm{Re}_s^{-0.25} \tag{12}$$

where $\mathrm{Re}_s = \rho_g V d_H / \mu$, is the Reynolds number for flow in the nozzle defined in terms of the helix swirl velocity. Eqs. (11) and (12) give ΔP, using Eqs. (6) and (9) to get l and d_H, respectively.

For flows in helical coils, however, several authors have published correlations for predicting the friction factor. The most popular are those of

Ito (1969):

$$f = 0.076\,\mathrm{Re}_s^{-0.25} + 0.00725\left(\frac{d_H}{d_2}\right)^{0.5} \tag{13}$$

and Srinivasan *et al.* (1970):

$$f = 0.084\left[\mathrm{Re}_s\left(\frac{d_H}{d_2}\right)^{-0.5}\right]^{-0.2} \tag{14}$$

where $\mathrm{Re}_s (d_H / d_2)^{0.5}$ is the Dean number, *Dn*, which characterises the magnitude of the secondary motion of flow through the toroidal passage, and d_H / d_2 is the coil curvature ratio, a characteristic dimensionless group which describes the geometry of the helical pipe.

Note that the helix friction factor relations have been changed from their original forms to conform to the geometry of the spiral nozzle used in this work. In the original formulations, fluid flow occurs inside a helical pipe wound around a central tube support (Fig. 3) whereas in this work the flow occurs outside the helical coil placed in a nozzle. d_H replaces the coil diameter (d_{coil}) where the flow occurs, while d_2 replaces d_{helix}, which is the diameter of the helix (Cozzini 2009; Hüttl and Friedrich 2000; Manlapaz and Churchill 1980).

In the present study, air at atmospheric conditions was used and the density and viscosity were assumed to be constant and taken as 1.2 kg/m^3 and 1.8×10^{-5} Pa s, respectively.

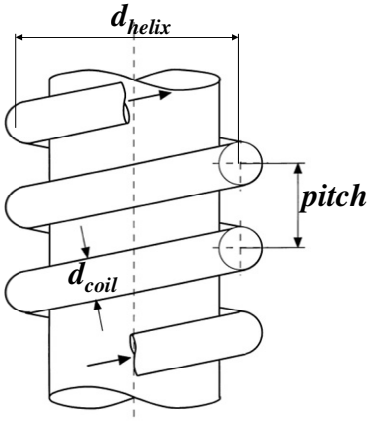

Fig. 3. Typical geometric configuration of a helically coiled pipe.

4. Results and discussion

Results obtained for the three different configurations of the fluidised bed are presented in this section. For each of the MR images, the areas of low signal intensity (i.e. black regions) correspond to a void or jet/bubble region where there are no particles while the areas of high intensity (i.e. white/grey regions) correspond to regions occupied by solid particles.

4.1. *Jet formation in the bed*

A series of 2D RARE images of the fluidised bed with the main bed unfluidised are presented in Fig. 4. Each row of images corresponds to nozzle gas velocities of between 1.3 m/s and 2.5 m/s. A jet structure similar to Fig. 2 can be observed to form at the nozzle, extending into the bed. The jets produced by the flush helix (top row) appear to be swirling in the bed and slightly deflected from the central axis while jets for the lowered helix and plain nozzle are axi-symmetric. It can be seen that the presence and position of the helix significantly affect the jet penetration depth (L_j), defined in Fig. 2. Fig. 5 shows the variation in jet length with gas flow rate for all three configurations. The measured length of the jet is highest when the helix is flush with the distributor while the jet lengths for the plain nozzle are intermediate between the flush spiral and the lowered helix, as shown in Fig. 5. It appears that when the helix is flush with the top of the distributor plate, the swirling effect produced by the centrifugal force of the helix stabilises the gas flow, producing a longer jet. As expected, the jet lengths increase with the nozzle gas velocity for all three cases. Merry's correlation for vertical jets (Eq. (1)) agrees more closely with the plain nozzle than with either the flush or lowered spiral. The difference between the measured and predicted jet lengths when the spiral is present may be caused by secondary flow.

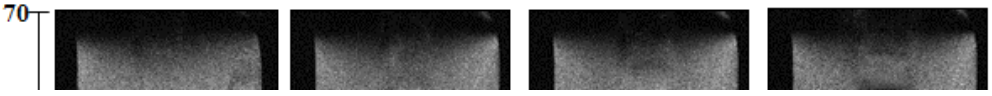

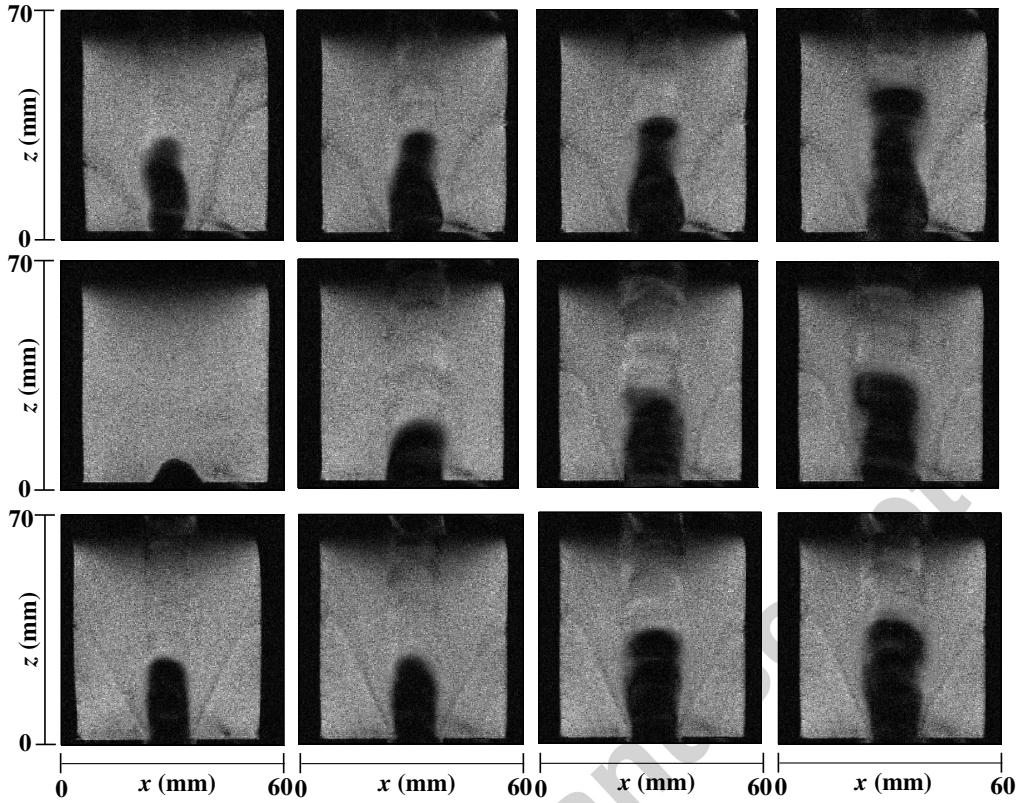

Fig. 4. RARE images of jets at different nozzle gas velocity, U_N (from left: 1.3 m/s, 1.7 m/s, 2.1 m/s and 2.5 m/s). Top row: nozzle with flush helix; middle row: nozzle with lowered helix; bottom row: plain nozzle. Note: the streaks seen in the images are artefacts due to the motion of the particulate phase; these should be ignored.

The *x*-*y* spin-echo intensity maps of the bed at a nozzle gas velocity of 1.7 m/s are shown in Fig. 6. It can be seen that the flush helix (a) produces the deepest penetrating jet, as evidenced by the characteristic void due to the jet remaining even at 30 mm above the distributor. The jet voids in the lowered helix (b) and plain nozzle (c) terminate at heights of around 20 mm and ~30 mm, respectively. These confirm the observations made earlier. Above these depths, the gas diffuses into the main bed.

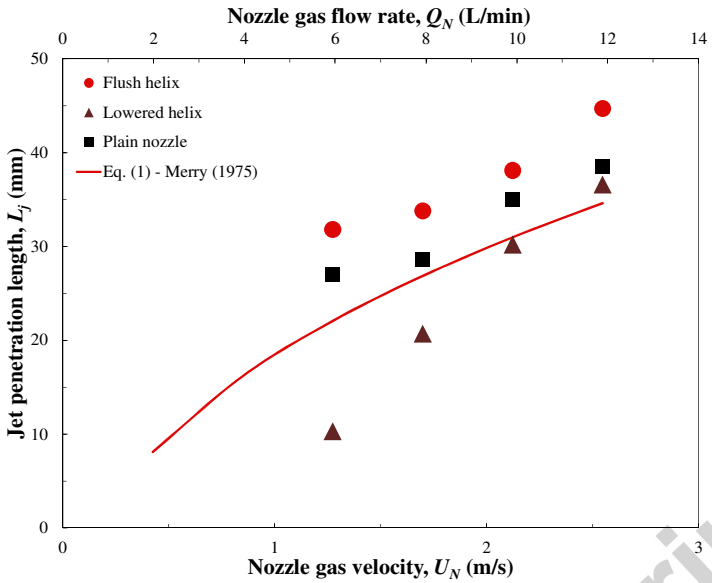

Fig. 5. Jet length for nozzles as a function of gas flow rate.

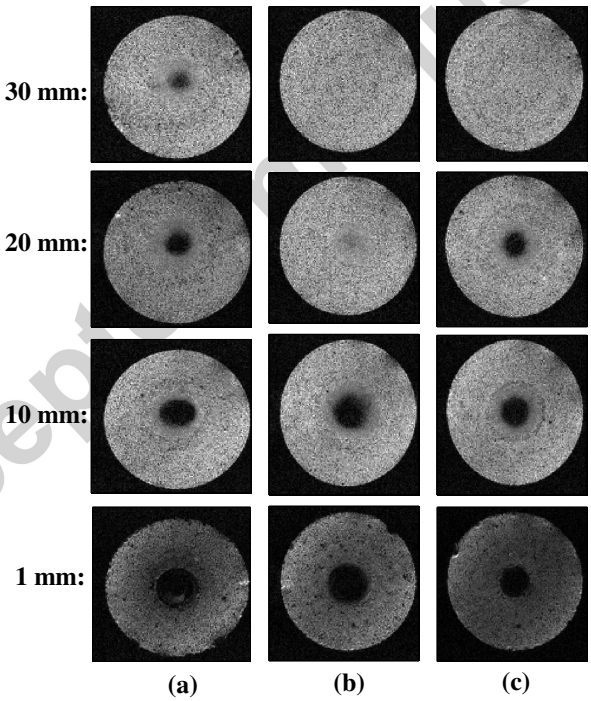

Fig. 6. Multislice (*x*-*y*) images showing signal intensity at different heights above the distributor for nozzle gas velocity, U_N, of 1.7 m/s (8 L/min). (a) nozzle with flush helix (b) nozzle with lowered helix (c) plain nozzle.

4.2. *Bubble formation in the bed*

The formation of bubbles was studied using FLASH and the resulting images are shown in Fig. 7 at nozzle gas velocity of 2.1 m/s for all three configurations. The FLASH images were

used because the RARE images, which showed the jets with high resolution, were susceptible to motion artefacts and could not be used to study bubbling fluidised beds. A time-series of images, covering 106 ms, shows the bubble build up process where a jet penetrates into the bed before the top breaks up into bubbles which rise through the bed and coalesce to form bigger bubbles. While bubbles detach almost at the distributor for the lowered helix, the height of bubble detachment from the jet with the flush helix and plain nozzle are about 30 mm and 20 mm above the nozzle exit, respectively. Thus it appears that the flush helix forms a more stable jet than the other two layouts. This further confirms the characteristics observed in Fig. 4.

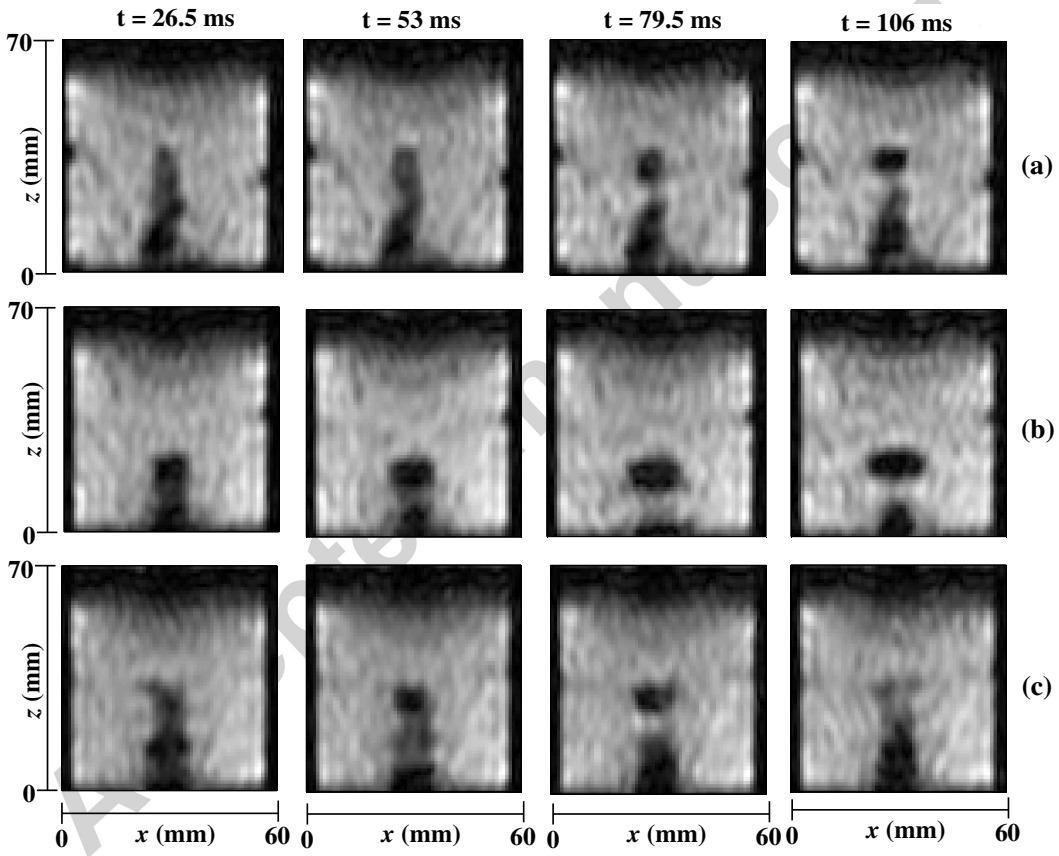

Fig. 7. MR images showing transition from jetting to bubbling at U_N of 2.1 m/s (10 L/min). Top row (a): flush helix; middle row (b): lowered helix; bottom row (c): plain nozzle.

Images of bubble formation at two gas velocities are presented in Fig. 8. Comparing the corresponding top and bottom images, it can be seen that the jet penetration length decreases while the bubble size increases with nozzle gas flow rate. This observation agrees with the two-phase theory (Grace and Clift 1974) which predicts larger bubbles at higher gas

velocities. At a nozzle gas velocity of 3.4 m/s, the bubble diameters are found to be 14.6±1.7 mm, 16.6±1.6 mm and 19.2±1.7 mm for the flush spiral, lowered spiral and plain nozzle respectively. These increased to 16.3±2.0 mm, 18.6±1.7 mm and 21.2±1.2 mm respectively at 4.2 m/s. The error is the standard deviation of the estimates from five observations in each case; the image pixel resolution is about 1.9 mm and this may be responsible for the observed variations in the bubble sizes. Merry's bubble size correlation (Eq. (2)) predicts values of 13.5 mm at 3.4 m/s and 14.7 mm at 4.2 m/s, which agree fairly well with the measured sizes. The bubble diameter d_b was estimated as the volume-equivalent diameter, defined as the diameter of a sphere of the same volume as the bubble; the bubble is assumed to be ellipsoidal and symmetrical about its vertical axis, hence

$$d_b = \sqrt[3]{a^2 b} \tag{15}$$

a and b being the width and height of a bubble in the image, respectively.

Using the ultra-fast MR images, the bubble diameters at different nozzle gas flow rates are computed. The equivalent spherical diameter, d_b, gives the bubble volume V_b, so

$$V_b = (\pi/6) d_b^3 \tag{16}$$

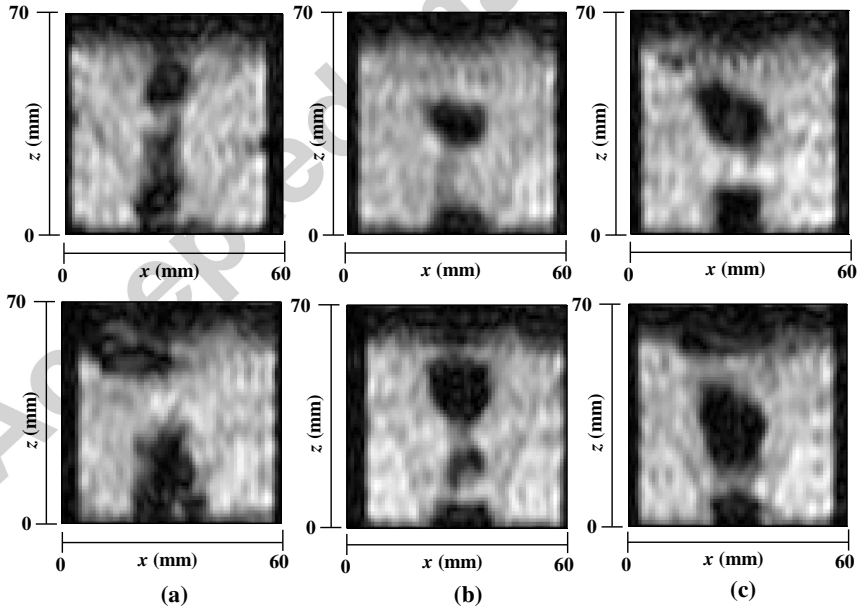

Fig. 8. Images of bed in full bubbling state. Top row at U_N of 3.4 m/s (16 L/min); bottom row at U_N of 4.2 m/s (20 L/min). (a) nozzle with flush helix (b) nozzle with lowered helix (c) plain nozzle.

The measured bubble volumes are compared to the bubble volumes estimated using the theory proposed by Davidson and Schüler (1960) for bubble formation in an inviscid liquid given by

$$V_b = 1.378 \frac{Q_N^{1.2}}{g^{0.6}} \tag{17}$$

where Q_N is the volumetric gas flow rate through the nozzle.

Fig. 9 compares the measured volume of detached bubbles from the jets with the volume calculated using Eq. (17) at different nozzle gas flow rates for the three fluidised bed configurations. It can be seen clearly that the plain nozzle produces bigger bubbles compared to the spiral nozzle, regardless of whether the helix is in either the flush or lowered position. This suggests that the swirling flow promotes smaller bubble formation under the same fluidising conditions with the excess gas dispersing into the particulate phase, thus enhancing lateral mixing. Furthermore, Fig. 9 shows that the Davidson and Schüler (1960) relation deviates significantly from the experimentally measured bubble volumes. This may be due to gas leakage into the dense phase during the process of bubble formation, which was not taken into account in the analysis. In the original work by Davidson and Schüler leading to Eq. (17), the main bed was incipiently fluidized separately.

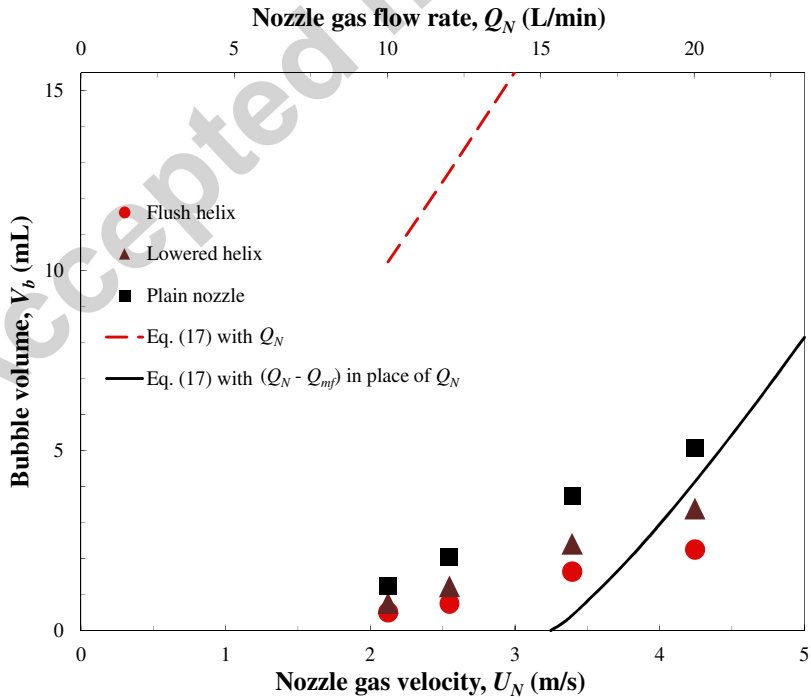

Fig. 9. Comparison between measured and predicted bubble volumes.

The observation in the present work implies that the flow rate of gas as bubbles is less than the inlet gas flow through the nozzle. Another possible reason for the deviation could be the different configuration and complex hydrodynamics of the fluidised bed investigated in this work. However, in the limiting case, assuming some of the nozzle gas flow goes into fluidising the particles in the main bed, and when Q_N in Eq. (17) is replaced by the volumetric flow rate through the nozzle in excess of that for minimum fluidisation, i.e. $(Q_N - Q_{mf})$ or $(U_N A_N - U_{mf} A_B)$, the agreement between the measured and predicted bubble volumes is much improved. For the gas flow rates range $10 < Q_N < 20$ L/min, the gas going into the particulate phase is finite but less than Q_{mf}.

4.3 *Frequency of bubble formation in the bed*

The frequency of bubble formation f_b is important when analysing the behavior of a fluidised bed. In this work, the frequencies of bubble formation were obtained by counting the total number of bubbles detaching from the top of each jet for each nozzle configuration using the ultra-fast magnetic resonance imaging videos and converting these to number of bubbles per second using the image acquisition time. Thus, these measurements were independent from those used to estimate the bubble size in Fig. 9, although they were derived from the same experimental data. The frequency of bubble formation can also be calculated from $f_b = Q_N / V_b$ with Eq. (17), giving

$$f_b = \frac{g^{0.6}}{1.378 Q_N^{0.2}} \tag{18}$$

Fig. 10 shows the measured bubble formation frequency. It is observed that the bubble frequency increases with gas flow rate for all three layouts in the range investigated. The plain nozzle has the highest bubble formation frequency at all flow rates compared to the flush and lowered spiral configurations. The smaller bubble formation frequencies observed with the helix may be due to an increase in gas flow entering the particulate phase.

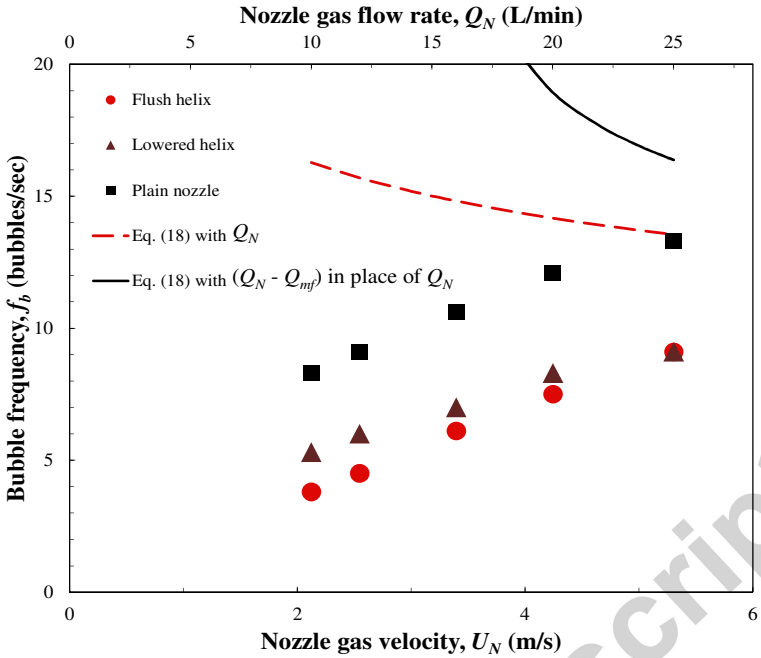

Fig. 10. Frequency of bubble formation for the nozzles.

The measured frequencies range between 3.8 and 13.3 Hz, in good agreement with the findings of Kunii and Levenspiel (1991) who reported that most published measurements of the frequency of bubble formation lie between 7 and 12 Hz. Since the plain nozzle forms larger bubbles and has somewhat higher bubble formation frequencies than the spiral nozzle, this implies that significantly more gas passes through the bed as bubbles, with possibly less contact with the particles. On the other hand, the spiral nozzle produces smaller and fewer bubbles (i.e. low bubble frequency), indicating that most of the gas is distributed into the dense phase of the bed thus promoting gas-solid contact.

It appears that the theoretical relations (Eqs. (17) and (18)) give, at high flow rates, the right order of magnitude of (*i*) observed bubble volume, Fig. 9, and (*ii*) observed bubble frequency, Fig. 10. This may be due to the fact that at high flow rates, the particulate phase is more fully fluidized. Thus the theoretical relations become more relevant. The differing trends in Fig. (10), i.e. actual frequency increases with flow rate whereas the theoretical frequency decreases with flow rate, may be due to the fact that the main bed was not separately fluidised. On balance, it seems better to assume that the volume entering the bubbles is $(Q_N - Q_{mf})$. Further experiments are needed with the main bed incipiently fluidised so that it would be reasonable to assume that all of the nozzle air goes into bubbles.

4.4 *Pressure drop across the swirling flow nozzle*

Fig. 11 shows the experimentally measured and theoretically calculated pressure drops across the nozzle, with and without the helix, as a function of the nozzle gas velocity U_N and flow rate Q_N. The theoretical predictions were obtained by substituting the friction factor correlations (Eqs. (12), (13) and (14)) into the pressure drop expression (Eq. (11)). It can be seen that, as might be expected, the pressure drops for the flush and lowered spiral nozzle configurations are significantly higher than for the plain nozzle. This clearly indicates that the toroidal geometry has a substantial influence on the flow characteristics. The higher pressure drop in the helical nozzle arises from two effects: first, the helical passage gives a longer path length and reduced cross-sectional area for flow, so that the flow velocity, V, in the spiral is much greater than the gas velocity through the nozzle, U_N. In addition, the secondary flow induced within the helical coil increases the frictional loss. At all gas flow rates, the results show that the pressure drop across the flush spiral is higher than that of the lowered spiral, the difference becoming larger at higher gas velocity. This is because the lowered spiral gives a larger exit diameter compared to the flush spiral, hence there is pressure recovery between the top of the lowered spiral and the distributor plate.

Comparing the experiment and theory using the turbulent flow friction factor correlations for coils (Eqs. (13) and (14)), Fig. 11 shows good agreement between the model predictions and the experimental data for the nozzle when the helix is flush with the top of the distributor for nozzle gas velocities up to about 10 m/s. Above this velocity there is a deviation between the experimentally measured and predicted values, which may be due to the effect of vibration and flow pulsation which were significant during experiments at higher gas velocities and made accurate pressure drop measurements more difficult. Unsurprisingly, the Blasius simple pipe model (Eq. 12) gives lower pressure drop predictions than the friction factor relations for helical coils (Eqs. (13) & (14)), but interestingly the Blasius equation correlates the pressure drops for the lowered helix fairly well up to a gas velocity of about 10 m/s.

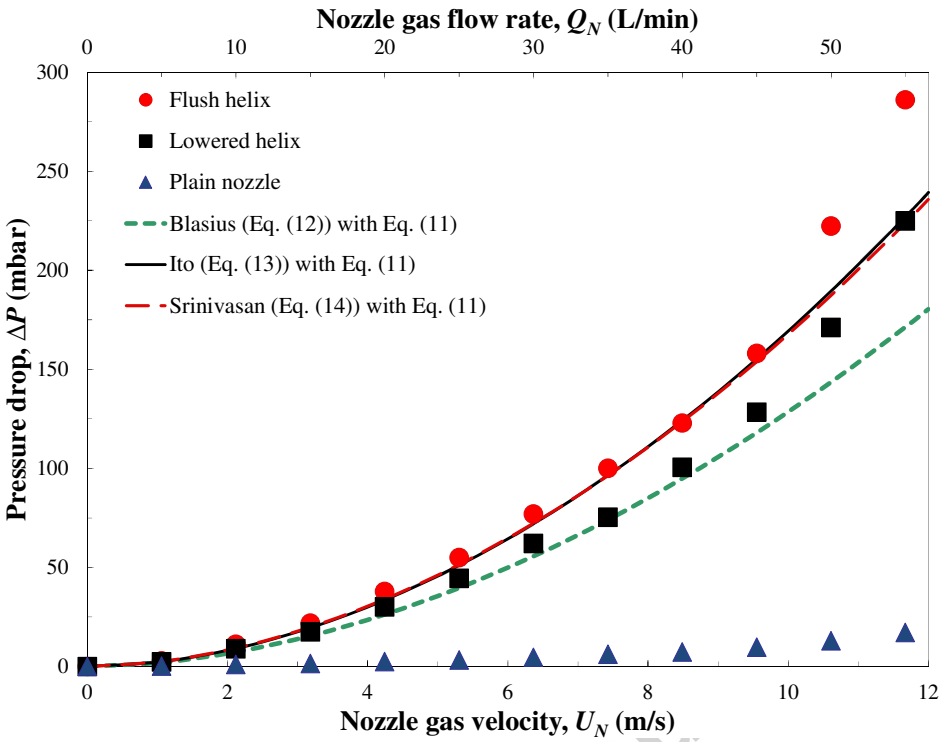

Fig. 11. Measured and predicted pressure drop across the nozzles.

5. Conclusions

In this work, a fluidised bed has been investigated with a novel gas distributor design containing a spiral helix, which makes the inlet gas swirl as it enters the bed. Magnetic resonance imaging allowed the visualization of the flow and mixing pattern in the bed which showed that the swirling flow nozzle produced better gas-solid contact compared to the simple nozzle. Smaller and less frequent bubbles were observed with the spiral helix, which suggests increased lateral gas dispersion into the dense phase. Pressure measurements indicate that the nozzle distributor containing a helix exhibits significantly higher pressure drop than the simple nozzle. This effect is caused by the swirling flow giving a higher velocity within the helix; an additional factor is secondary flow which increases the friction factor. Results also showed that the position of the helix within the nozzle significantly affects the flow characteristics and performance of the bed. Overall, the swirling flow nozzle with a lowered helix would give the best performance since it produces a reasonably good hydrodynamic behaviour in addition to lower pressure drop compared to the flush helix. A distributor with multiple swirling flow nozzles ('tuyeres') is feasible for an industrial fluidised bed and would produce improved fluidisation characteristics, but the improvement

needs to be balanced against higher capital and operating costs, the latter due to energy consumption for air supply to the bed.

Acknowledgements

The authors thank Dr Stephen Sutcliffe and Mo Dadvar of Huntsman for providing both financial and technical assistance for this project, and Suttons Seeds for the kind donation of poppy seeds used for MRI. S.M. Aworinde is grateful to the Cambridge Commonwealth Trust (CCT) for scholarship award to study at Cambridge.

Notation

a	Width of bubble, m
A	Spiral flow area, m^2
A_B	Whole bed cross-sectional area, m^2
A_N	Plain nozzle cross-sectional area, m^2
b	Height of bubble, m
d_b	Equivalent diameter of bubble, m
d_{coil}	Diameter of helical coil, m
d_H	Hydraulic mean diameter, m
d_{helix}	Diameter of helix, m
d_p	Particle diameter, m
d_1	Helix core diameter, m
d_2	Helix outer diameter, m
d_3	Nozzle diameter, m
Dn	Dean number = $\mathrm{Re}_s (d_H / d_2)^{0.5}$
f	Friction factor for helical coil
f'	Helix flight, m
f_b	Bubble formation frequency, bubbles/sec
g	Acceleration due to gravity, m/s^2
l	Length of spiral, m
L_j	Jet penetration length, m
n	Number of turns in the helix
p	Helix pitch, m
P'	Spiral wetted perimeter, m
ΔP	Pressure drop across nozzle, mbar
Q_N	Gas flow rate through the nozzle, L/min
Q_{mf}	Gas flow rate corresponding to minimum fluidisation velocity, L/min
Re	Reynolds number
Re_s	Reynolds number for flow in spiral nozzle = $\rho_g V d_H / \mu$
T_E	Echo time, ms
T_R	Repetition time, ms
U_{mf}	Minimum fluidisation velocity, m/s
U_N	Gas velocity through nozzle, m/s

V Tangential gas velocity within the spiral helix, m/s
V_b Bubble volume, mL
x,y,z Cartesian coordinate system

Greek letters

ρ_g Gas density, kg/m^3
ρ_p Particle density, kg/m^3
μ Viscosity, Pa s
θ Jet half angle, deg
φ Helix inclined angle, deg

References

Blasius, P.R.H. 1913. "Das Aehnlichkeitsgesetz Bei Reibungsvorgangen in Flüssigkeiten." *Forschungshef* 131: 1–41.

Chen, R.C., and L.-S. Fan. 1992. "Particle Image Velocimetry for Characterizing the Flow Structure in Three-Dimensional Gas-Liquid-Solid Fluidized Beds." *Chem. Eng. Sci.* 47: 3615–22.

Choi, J.H., J.E. Son, and S.D. Kim. 1988. "Bubble Size and Frequency in Gas Fluidized Beds." *J. Chem. Eng. Jpn.* 21 (2): 171–78.

Chyang, C-S., and Y-C. Lin. 2002. "A Study in the Swirling Fluidizing Pattern." *J. Chem. Eng. Jpn.* 35: 503–12.

Cozzini, M. 2009. "Helical Coil Flow: A Case Study." In *COMSOL Conference*. Milan.

Davidson, J.F., and B.O.G. Schüler. 1960. "Bubble Formation at an Orifice in an Inviscid Liquid." *Trans. Inst. Chem. Eng.* 38: 335–42.

De Wilde, J., and A. de Broqueville. 2008. "Experimental Investigation of a Rotating Fluidized Bed in a Static Geometry." *Powder Technol.* 183 (3): 426–35.

Dean, W.R. 1927. "Streamline Motion of Fluid in a Curved Pipe." *Phil. Mag.* 5: 673–95.

Dunn, W.E. 1958. "Charging Fluidizing Gas into Fluidized Bed Reactor." *U.S. Patent 2,856,264 to DuPont*.

Dyakowski, T., R.B. Edwards, C.G. Xie, and R.A. Williams. 1997. "Application of Capacitance Tomography to Gas-Solid Flows." *Chem. Eng. Sci.* 52: 2099–2110.

Geldart, D. 1973. "Types of Gas Fluidization." *Powder Technol.* 7: 285–92.

Grace, J.R., and R. Clift. 1974. "On the Two-Phase Theory of Fluidization." *Chem. Eng. Sci.* 29: 327–34.

Hüttl, T.J., and R. Friedrich. 2000. "Influence of Curvature and Torsion on Turbulent Fow in Helically Coiled Pipes." *Int. J. Heat Fluid Flow* 21 (3): 345–53.

Ito, H. 1969. "Laminar Flow in Curved Pipes." *Z. Agnew. Math. Mech.* 49: 653–63.

Kim, J., and G.Y. Han. 2006. “Effect of Agitation on Fluidization Characteristics of Fine Particles in a Fluidized Bed.” *Powder Technol.* 166 (3): 113–22.

Kleinfelder, E.O. 1969. “Fluidizing Gas Introduction into a Reactor.” *U.S. Patent 3,475,117 to DuPont*.

Koksal, M., and H. Vural. 1998. “Bubble Size Control in a Two-Dimensional Fluidized Bed Using a Moving Double Plate Distributor.” *Powder Technol.* 95: 205–13.

Kunii, K., and O. Levenspiel. 1991. *Fluidization Engineering*. 2nd ed. Newton, MA: Butterworth-Heinemann.

Manlapaz, R.L., and S.W. Churchill. 1980. “Fully Developed Laminar Flow in a Helically Coiled Tube of Finite Pitch.” *Chem. Eng. Commun.* 7: 57–78.

Mantle, M.D., A.J. Sederman, L.F. Gladden, J.M. Huntley, T.W. Martin, R.D. Wildman, and M.D. Shattuck. 2008. “MRI Investigations of Particle Motion within a Three-Dimensional Vibro-Fluidized Granular Bed.” *Powder Technol.* 179 (3): 164–69.

Mathur, K.B., and N. Epstein. 1974. *Spouted Beds*. New York: Academic Press, Inc.

Mawatari, Y., Y. Tatemoto, and K. Noda. 2003. “Prediction of Minimum Fluidization Velocity for Vibrated Fluidized Bed.” *Powder Technol.* 131 (1): 66–70.

Menon, N. 1997. “Diffusing-Wave Spectroscopy of Dynamics in a Three-Dimensional Granular Flow.” *Science* 275 (5308): 1920–22.

Merry, M.D. 1975. “Penetration of Vertical Jets into Fluidized Beds.” *AIChE J.* 21 (3): 507–10.

Müller, C.R., D.J. Holland, A.J. Sederman, M.D. Mantle, L.F. Gladden, and J.F. Davidson. 2008. “Magnetic Resonance Imaging of Fluidized Beds.” *Powder Technol.* 183 (1): 53–62.

Ouyang, F., and O. Levenspiel. 1986. “Spiral Distributor for Fluidized Beds.” *Ind. Eng. Chem. Process Des. Dev.* 25: 504–7.

Pore, M., T.C. Chandrasekera, D.J. Holland, A. Wang, F. Wang, Q. Marashdeh, M.D. Mantle, et al. 2012. “Magnetic Resonance Studies of Jets in a Gas–solid Fluidised Bed.” *Particuology* 10 (2): 161–69.

Pore, M., D.J. Holland, T.C. Chandrasekera, C.R. Müller, A.J. Sederman, J.S. Dennis, L.F. Gladden, and J.F. Davidson. 2010. “Magnetic Resonance Studies of a Gas–solids Fluidised Bed: Jet–jet and Jet–wall Interactions.” *Particuology* 8 (6): 617–22.

Rowe, P.N. 1971. “Experimental Properties of Bubbles.” In *Fluidization*, edited by J.F. Davidson and D. Harrison, 121–91. New York: Academic Press.

Shu, J., V.I. Lakshmanan, and C.E. Dodson. 2000. “Hydrodynamic Study of a Toroidal Fluidized Bed Reactor.” *Chem. Eng. Process.* 39: 499–506.

Sobrino, C., A. Acosta-Iborra, D. Santana, and M. de Vega. 2009. “Bubble Characteristics in a Bubbling Fluidized Bed with a Rotating Distributor.” *Int. J. Multiphase Flow* 35 (10). Elsevier Ltd: 970–76.

Sreenivasan, B., and V.R. Raghavan. 2002. "Hydrodynamics of a Swirling Fluidised Bed." *Chem. Eng. Process.* 41: 99–106.

Srinivasan, P.S., S.S. Nandapurkar, and S.S. Holland. 1970. "Friction Factors for Coils." *Trans. Inst. Chem. Eng.* 48: 156–61.

Stein, M., T.W. Martin, J.P.K. Seville, P.A. McNeil, and D.J. Parker. 1997. "Positron Emission Particle Tracking: Particle Velocities in Gas Fluidised Beds, Mixers and Other Applications." In *Noninvasive Monitoring of Multiphase Flows*, edited by J. Chaouki, F. Larachi, and M.P. Dudukovic, 161–84. Amsterdam: Elsevier.

Thangam, S., and N. Hur. 1990. "Laminar Secondary Flow through a Closely Coiled Pipe." *J. Fluid. Mech.* 217: 421–40.

Thomson, J. 1876. "On the Origin of Windings in Rivers in Alluvial Plains, with Remarks on the Flow of Water Round Bends in Pipes." *Proc. R. Soc. Lond.* 25: 5–8.

Wen, C.Y., N.R. Deole, and L.H. Chen. 1982. "A Study of Jets in a Three-Dimensional Gas Fluidized Bed." *Powder Technol.* 31: 175–84.

Werther, J. 1974. "Bubbles in Gas Fluidised Beds." *Trans. Inst. Chem. Eng.* 52: 149–59.

Graphical abstract

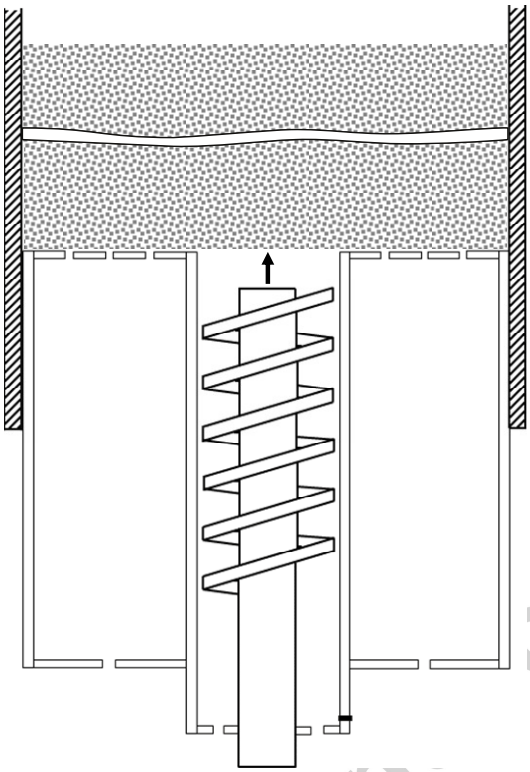

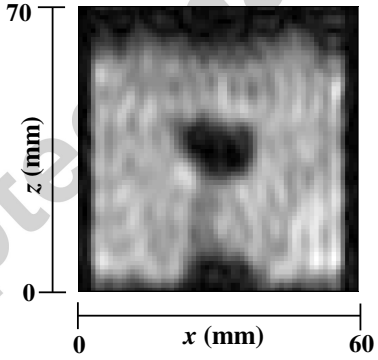

Highlights

- Hydrodynamics and pressure drop of a swirling flow nozzle distributor investigated
- Swirl promotes lateral dispersion of gas and better gas-solid contact in fluidised bed
- Pressure drop across nozzle containing the spiral significantly higher than plain nozzle
- Measured properties of the nozzle reasonably agree with theoretical predictions